Electrochimica Acta 111 (2013) 755–761

Contents lists available at ScienceDirect

Electrochimica Acta

journal homepage: www.elsevier.com/locate/electacta

Efficiency enhancement of TiO_2 nanodendrite array electrodes in $CuInS_2$ quantum dot sensitized solar cells

Zhuoyin Peng[a,1], Yueli Liu[a,1], Yinghan Zhao[a], Wei Shu[a], Keqiang Chen[a], Qiaoliang Bao[b], Wen Chen[a,*]

[a] State Key Laboratory of Advanced Technology for Materials Synthesis and Processing, and School of Materials Science and Engineering, Wuhan University of Technology, Wuhan 430070, PR China
[b] Department of Materials Engineering, Monash University, Clayton, Victoria 3800, Australia

ARTICLE INFO

Article history:
Received 4 April 2013
Received in revised form 15 August 2013
Accepted 15 August 2013
Available online 23 August 2013

Keywords:
TiO_2 nanodendrite arrays
$CuInS_2$ quantum dots
Electron injection
Efficiency enhancement

ABSTRACT

Single crystal three-dimensional TiO_2 nanodendrite arrays were prepared by a hydrothermal process, which were successfully sensitized with $CuInS_2$ quantum dots as photo-anodes to fabricate the solar cells. The UV–vis absorption and photoluminescence spectra observe that the TiO_2 nanodendrite based photo-anode structures are more efficient to improve the optical absorption properties and electron–hole separation. Electrochemical impedance spectra and photoluminescence decay analysis indicate that the TiO_2 nanodendrite based solar cells structure have higher electron injection rate. Under full sunlight illumination, the $CuInS_2$ quantum dot sensitized TiO_2 nanodendrite arrays exhibit a photovoltaic power conversion efficiency of 1.26%, which has great improvement of J_{SC} comparing with that of $CuInS_2$ quantum dot sensitized with TiO_2 nanoparticles and nanorods.

1. Introduction

Quantum dot-sensitized solar cells (QDSSCs) have been received much attention in fabricating the next generation photovoltaic devices [1]. The quantum dots (QDs) such as CdS, CdSe, CdTe, PbS and $CuInS_2$ have been recognized to provide the opportunities for light absorption in the whole solar spectrum region because of their unique physical properties of tuning the absorption edge with the size, ultrafast electron transfer, and multiple excitons generation (MEG) [2–8]. Among these semiconductor QDs, $CuInS_2$ with direct band gap can effectively improve the photovoltaic performance of QDSSCs due to its high absorption coefficient, which is well matched with the full solar spectrum [9–11]. Recently, the photovoltaic efficiency of the $CuInS_2$ QDSSCs has been gradually improved, such as, the efficiency of $CuInS_2$ QDSSCs is over 0.7% in our previous work [12], and Kamat's group has fabricated the $CuInS_2$ QDSSCs with the efficiency of 1.19% [13]. Moreover, it is also employed with CdS QDs to fabricate the quantum dots co-sensitized solar cells, which can obtain the higher photovoltaic efficiency [13–15]. However, the photovoltaic performance of $CuInS_2$ QDSSCs is still needed to be improved.

Recently, TiO_2 nanomaterials have been widely used in solar cells due to their high stability, low cost, non-toxic and optical properties [16–19]. The TiO_2 nanoparticles (NPs) film with high surface area is always employed to be the basic photo-anodes of the QDSSCs, which have received some good results [20]. However, the electron mobility in the TiO_2 NPs film is much lower than that of the single crystal due to the electron trapping at grain boundaries. Additionally, with the increasing of QDs content, the TiO_2 NPs will gradually desquamate from the substrate, which induces the decrease of stability of the TiO_2 NPs film [21]. As a result, to further increase the photovoltaic performance of QDSSCs, it will be necessary to use single crystal nanostructured photo-anodes. One-dimensional TiO_2 nanostructures such as nanowires (NWs), nanorods (NRs) and nanotubes (NTs) have been employed to be photo-anodes due to the enhancement in electron–hole separation and electrons transport [22–25]. It can be efficient to improve the photovoltaic performance of QDSSCs. QDSSCs with these single crystal TiO_2 NRs, NWs and NTs have performed better photovoltaic efficiency in solar cells than that of TiO_2 NPs [26]. However, TiO_2 NRs, NWs and NTs photo-anodes have smaller surface areas than TiO_2 NPs photo-anodes, which will reduce the deposition content of the QDs to influence the generation of the photo-induced electrons. Instead of the TiO_2 NRs/NWs, the single crystal nanodendrites (NDs) with three-dimensional tree-like structures have larger surface areas for QDs sensitization to increase the electrons generation. Additionally, although these TiO_2 NDs are fabricated as photo-anodes to enhance the photovoltaic efficiency of

* Corresponding author. Tel.: +86 27 8765 1107; fax: +86 27 8776 0129.
E-mail address: chenw@whut.edu.cn (W. Chen).
[1] These authors contributed equally to this study and share first authorship.

0013-4686/$ – see front matter © 2013 Elsevier Ltd. All rights reserved.
http://dx.doi.org/10.1016/j.electacta.2013.08.054

dye-sensitized solar cells, there is little report on the photo-anode of QDSSCs [27]. Therefore, the investigation for developing the TiO_2 NDs based QDSSCs has become increasingly important.

In this paper, single crystal three-dimensional TiO_2 NDs arrays were synthesized by a hydrothermal process. And that were sensitized with $CuInS_2$ QDs to fabricate the QDSSCs. Moreover, the TiO_2 NPs and NRs were also used to compare the photovoltaic performance with the TiO_2 NDs. In addition, the ZnSe coating layer and the annealing post-treatment will also help to improve the electron injection [28,29]. The results indicate that the use of TiO_2 NDs array structure has higher current density than that of NPs and NRs. The QDSSCs based on the $CuInS_2$ QDs sensitized TiO_2 NDs solar cells effectively improved its photovoltaic performance.

2. Experimental

2.1. Materials

Copper (I) iodide ($CuI{\cdot}2H_2O$, 99.9%), indium (III) acetate ($InAc_3{\cdot}4H_2O$, 99%), 3-mercaptopropionic acid (MPA, 98%), titanium (IV) isopropoxide ($C_{12}H_{28}O_4Ti$, 98%) were purchased from Alfa-Aesar (Ward Hill, USA). Thiourea ($CS(NH_2)_2$, 98%), sulfur powder (S, 99%), sodium sulfur (Na_2S, 98%), hydrochloric acid (HCl, 36.5–38% by weight) and sodium hydroxide (NaOH, 96%) were purchased from Sinopharm Group Chemical Reagent Co., Ltd. (China). Methanol (HPLC grade), sulfur acid (ACS grade) and ethanol (99.5%) were purchased by Sinopharm Group Chemical Reagent Co., Ltd. (China). All the materials were directly used without further purification.

2.2. Preparation of TiO_2 electrodes

The TiO_2 nanodendrite arrays were prepared by hydrothermal method on the FTO conducting glass [27]. In a typical synthesis, 30 ml of concentrated hydrochloric acid was mixed with 30 ml of deionized water. 1 ml titanium isopropoxide was added dropwise in the mixture under vigorous stirring. The stirring was continued for 30 min at room temperature. After transferring the mixture into the Teflon-lined stainless steel autoclave (125 ml volume), some pieces of FTO substrates, which are ultrasonically cleaned for 60 min in a mixture solution of deionized water, acetone and ethanol with volume ratios of 1:1:1, were placed at an angle against the wall of the Teflon liner with the conductive side facing down. The hydrothermal synthesis was conducted at 150 °C for 20 h in an electric oven. After synthesis, the FTO substrate was taken out, rinsed extensively with deionized water, and allowed to be dried in ambient air. In order to increase the length of TiO_2 NRs, the as-prepared TiO_2 nanorod arrays were introduced with the similar solution except for the addition of 5 ml saturated NaCl solution at the same hydrothermal temperature for another 20 h. This process repeated two times to obtain the desired length of TiO_2 nanorod. After that, the TiO_2 nanorod arrays were conducted in the solution of 0.5 M 40 ml HCl and 2 ml titanium isopropoxide at 95 °C for 4 h. Another 2 h hydrothermal process with the same precursor solution was carried out for the branch growth on the TiO_2 nanorods. Finally the as-prepared TiO_2 nanodendrite arrays were washed with deionized water and then calcined at 450 °C for 30 min. For comparison, the anatase and rutile TiO_2 nanoparticles (NPs) photo-anodes with the thickness of 6 μm were prepared as our previous report [12].

2.3. Preparation of TiO_2/$CuInS_2$ photo-anodes

The MPA-capped $CuInS_2$ QDs of 3.5 nm were prepared according to previously reported method [12]. $CuInS_2$ quantum dots were linked to nanorods and nanodendrites using MPA as a linking agent, and the TiO_2 nanoparticle photo-anodes were also introduced to a contrast. Typically, after introduced to a pH 2 hydrochloric acid solution for 5 min, the TiO_2 nanodendrite array films were immersed in a MPA (1 M) and sulfur acid (0.1 M) acetonitrile solution for 12 h [30]. The films were then immersed in the MPA-capped $CuInS_2$ QDs methanol solution for 24 h after rinsing with acetonitrile and methanol. Such immerse process was repeated for several times to obtain the best photovoltaic properties (as shown in Figs. S1-S2 and Table S1). All the electrodes were coated by the ZnSe passivation coating, which is prepared by the SILAR method consisting of three dipping cycles in the 0.1 M $Zn(acac)_2$ and 0.1 M Se precursor solution prepared by selenium oxide and sodium borohydride for 1 min each dip to enhance the photovoltaic performance (as shown in Figs. S2-S4 and Table S1). Finally, the sensitized electrodes were annealing in Ar atmosphere at 300 °C for 5 min.

2.4. Fabrication of QDSSCs

After preparing the $CuInS_2$ QDs sensitized TiO_2 photo-anodes by above process, the solar cells were fabricated with the Cu_2S counter electrode by using a Surlyn thermoplastic frame. A standard redox polysulfide electrolyte was prepared by dissolving 0.5 M Na_2S, 2 M S, and 0.2 M KCl in water/methanol (7:3 by volume) solution, which was introduced into the sealed solar cells through a hole pre-drilled in the counter electrode. The active area of the solar cells was 0.16 cm^2.

2.5. Characterization and measurements

The crystal structures and morphologies of the TiO_2 and QDs were characterized by using X-ray diffraction (XRD, Pert-Pro, PANalytical, Netherlands), scanning electron microscope (FESEM, JSEM-5610LV, Japan) equipped with an energy dispersive spectrometer (EDS), and the high-resolution transmission electron microscope (TEM, JEM-2100F, JEOL, Japan). UV–vis absorption spectra (UV-2550, Shimadzu, Japan) and photoluminescence spectra (FS-2400, Shimadzu, Japan) were used to characterize the absorption edge and excited peak of QDs sensitized TiO_2 nanorod/nanodendrite array films. Full sun conversion efficiency was characterized by the Keithley 4200 semiconductor characterization system (Keithley Instruments, USA) under AM 1.5 condition (Newport 91160, 300 W xenon lamp, USA). The light intensity was determined using a reference monocrystalline silicon cell system (Oriel, USA). The incident photon to current conversion efficiency (IPCE) was measured using Newport's IPCE Measurement Kit (Crowntech, Q Test Station Series, USA), where a monochromator was used to obtain the monochromatic light from a 300 W Xe lamp (Newport). The photoluminescence decay was measured using time-resolved fluorescence spectroscopy (HORIBA Fluoromax-4, France).

3. Results and discussion

3.1. Structures and morphologies

The structures of TiO_2 NDs array films used as photo-anodes before and after $CuInS_2$ QDs sensitization are also illustrated by X-ray diffraction spectrometer (Fig. 1a). The XRD pattern of pure TiO_2 NDs is matched well with the standard pattern of rutile TiO_2 phase (JCPDS NO: 76-1941). After sensitized with $CuInS_2$ QDs, two extra peaks with (1 1 2) and (0 2 0) crystal planes appear at 2θ values of 32.52° and 37.82° from the tetragonal $CuInS_2$ phase (JCPDS NO: 85-1575), respectively, which clearly suggests the $CuInS_2$ QDs adsorption process.

Fig. 1b and c shows the field-emission scanning electron microscopy (FESEM) images of TiO_2 NRs arrays, the top view of

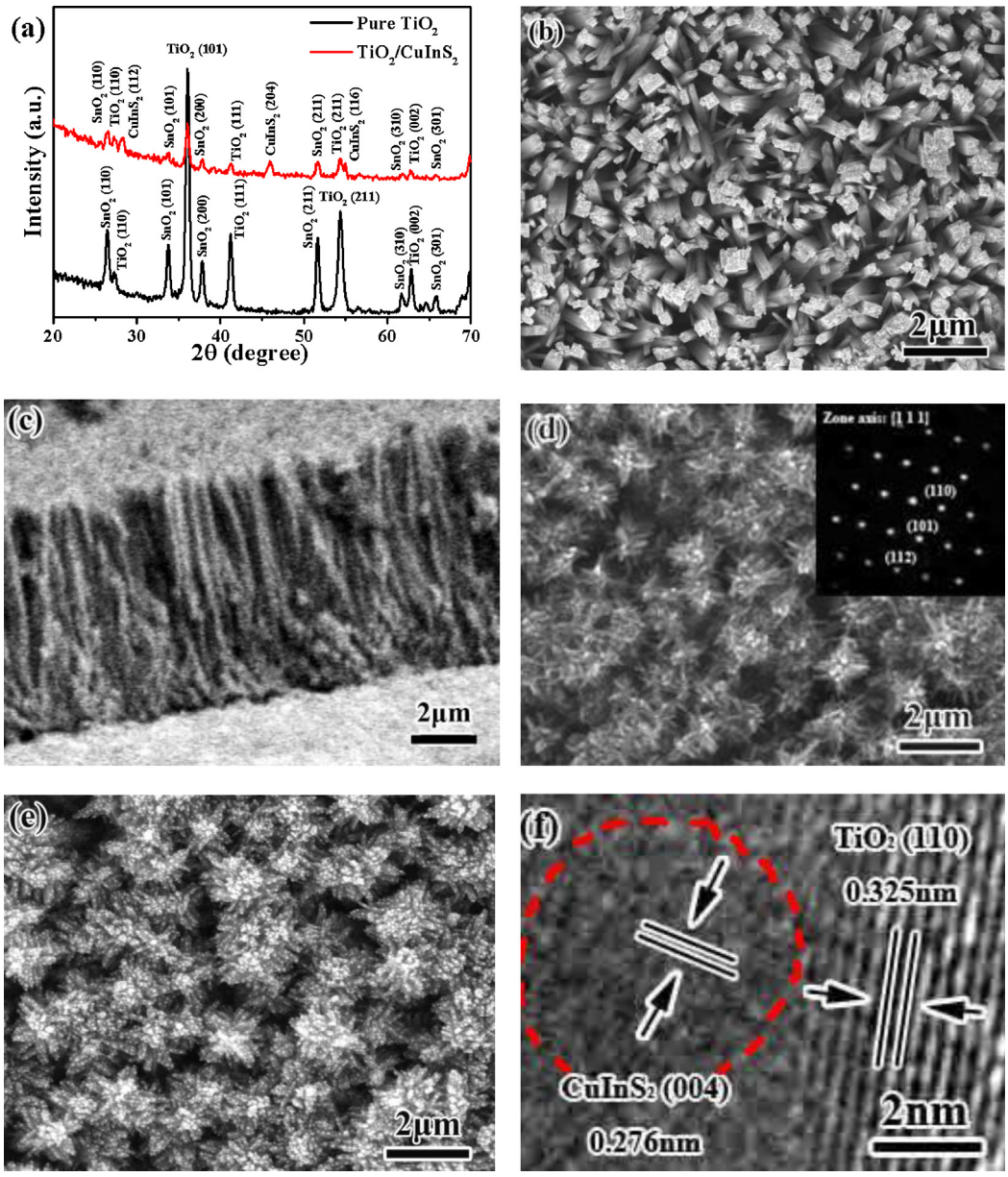

Fig. 1. Structures and morphologies of as-prepared materials: (a) XRD patterns; FESEM images of TiO_2 nanorod arrays at (b) top view and (c) cross-sectional view; FESEM images of TiO_2 nanodendrite arrays at (d) pure and (e) as-sensitized by $CuInS_2$ QDs; (f) HRTEM image of $CuInS_2/TiO_2$ NDs photo-anode.

FESEM image of the typical TiO_2 NRs is square and contains many step edges, which shows that the expected growth is from the substrate to form a tetragonal crystal. It also can be seen that the length of TiO_2 NRs is about 6 μm, and the average diameter is about 200 nm from the cross-sectional view of FESEM image of the TiO_2 NRs.

The NDs arrays are successfully prepared by the second step of the hydrothermal process as shown in Fig. 1d. To compare with TiO_2 NRs from FESEM images, the branches with the diameter of 20–30 nm and length of 120–150 nm are successfully prepared on the TiO_2 NRs, which can effectively increase the surface area ratio of TiO_2 films. This kind of branches with the same single crystal as the TiO_2 NRs will not consumedly reduce the possibility of electron trapping in TiO_2 photo-anodes. And the corresponding SAED pattern obviously indicates a single crystal structure of the TiO_2 NDs. Moreover, an increased amount of $CuInS_2$ QDs can be adsorbed on TiO_2 NDs due to the enlarged surface area ratio from the branches in the TiO_2 NDs. The surface feature of the TiO_2 NDs becomes roughness after $CuInS_2$ QDs sensitization, as shown in Fig. 1e. This actually indicates that the more content of $CuInS_2$ QDs can be adsorbed on the TiO_2 NDs than on the TiO_2 NRs. The typical HRTEM image of as-prepared $CuInS_2$ QDs sensitized TiO_2 NDs films is shown in Fig. 1f. It can be seen that $CuInS_2$ QDs with the diameter of about 3.5 nm are adsorbed on the TiO_2 NDs surface. And the observed lattice fringes of 0.325 nm and 0.276 nm are corresponding to the (1 1 0) crystal plane of rutile TiO_2 and the (2 1 4) crystal plane of $CuInS_2$ QDs, respectively.

3.2. UV–vis absorption and photoluminescence analysis

The absorption and photoluminescence spectra of TiO_2 NRs/$CuInS_2$ QDs/ZnSe (TRs), TiO_2 NDs/$CuInS_2$ QDs/ZnSe (TDs), anatase TiO_2 NPs/$CuInS_2$ QDs/ZnSe (a-TPs) and rutile TiO_2 NPs/$CuInS_2$ QDs/ZnSe (r-TPs) are shown in Fig. 2. Comparing with the different $TiO_2/CuInS_2$/ZnSe photo-anodes in Fig. 2a, the TiO_2 NDs sensitized photo-anodes have larger ultraviolet and visible light absorption edge than the TiO_2 NPs and TiO_2 NRs. It is actually

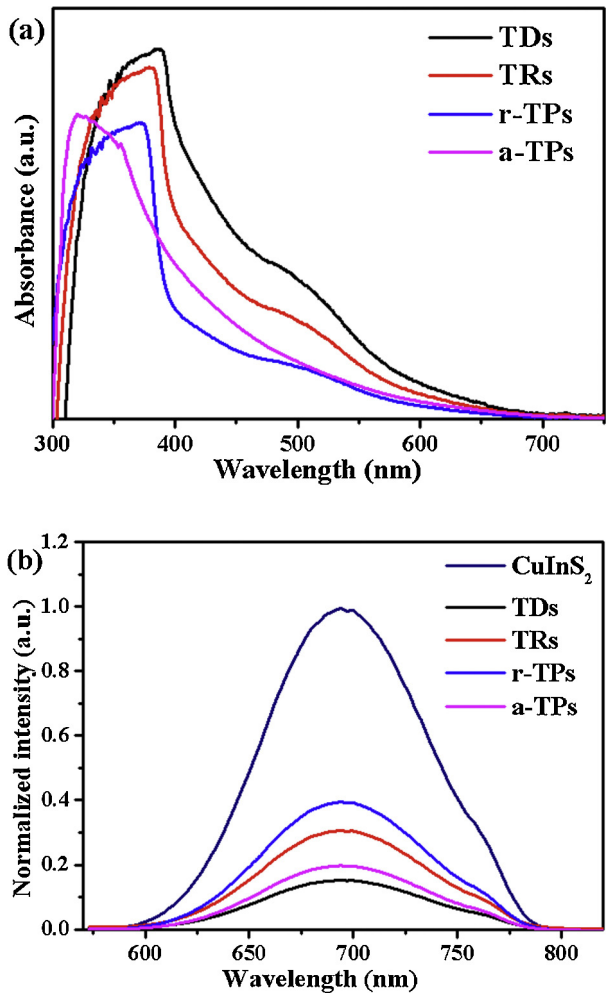

Fig. 2. (a) UV–vis spectra of different TiO_2/$CuInS_2$/ZnSe photo-anodes and (b) photoluminescence spectra of different TiO_2/$CuInS_2$/ZnSe photo-anodes.

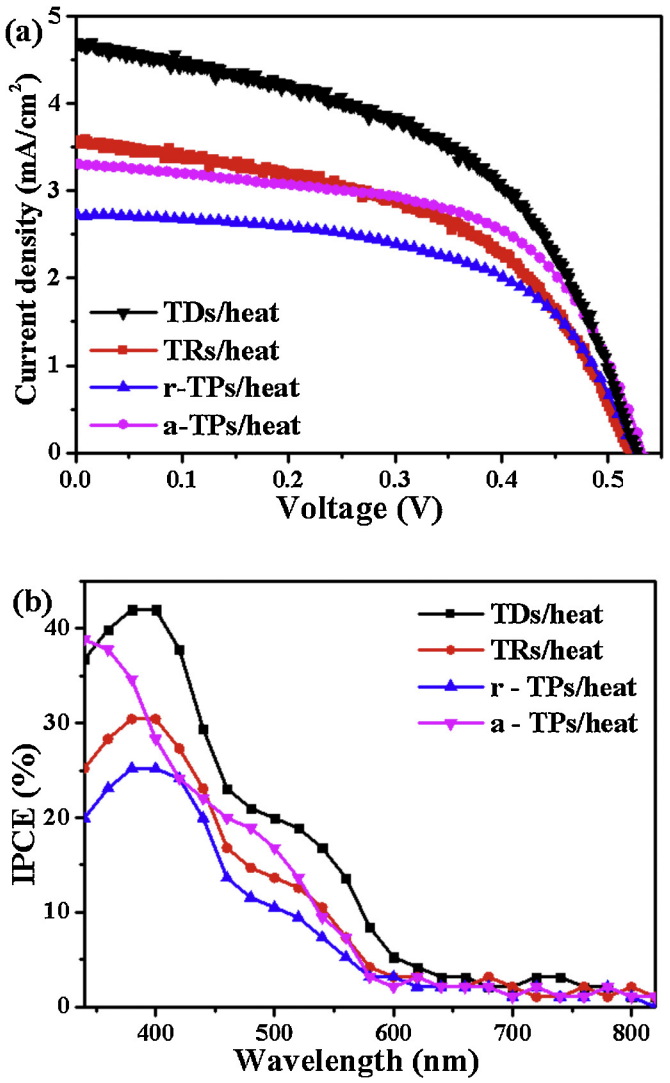

Fig. 3. (a) EIS spectra of $CuInS_2$ QDs sensitized solar cells with different TiO_2 photo-anodes and (b) photoluminescence decay of each device.

attributed to higher surface area of this TiO_2 NDs, which can adsorb more $CuInS_2$ QDs to improve the visible light absorption.

The photoluminescence spectra in Fig. 2b suggest that the $CuInS_2$ sensitizer has a photoluminescence peak at 700 nm, which is estimated that the size of these QDs to be 3.5 nm [31]. Due to the sensitization of $CuInS_2$ QDs, the photo-excited electrons in $CuInS_2$ QDs will transfer to TiO_2 to achieve an effective separation for the photo-excited electron–hole pairs, which induces that the photoluminescence peak of $CuInS_2$ QDs sensitized TiO_2 photo-anodes are seriously quenched comparing with that of the pure $CuInS_2$ QDs. Moreover, the lower photoluminescence peak intensity of TiO_2 NDs sensitized photo-anodes suggests the less photo-excited electron–hole pair recombination. It is clearly verified that this ordered three-dimensional single crystal TiO_2 NDs have the highest effective separation for the photo-excited electron–hole pairs.

3.3. Photovoltaic performance of QDSSCs

At least 20 devices have been measured to confirm the photovoltaic performance influence of TRs, TDs, a-TPs and r-TPs solar cells, and the average values of the *J–V* curve and photovoltaic parameters are shown in Fig. 3a and Table 1. It can be seen that the TRs (3.59 mA/cm^2) and TDs (4.70 mA/cm^2) photo-anodes with their well-aligned and single crystal structure have higher J_{SC} value than both r-TPs (2.74 mA/cm^2) and a-TPs (3.30 mA/cm^2) based solar cells. Even the TDs based solar cells are obviously higher than those of a-TPs based solar cells, which results in the photovoltaic power conversion efficiency of the former (1.26%) higher than the latter (1.00%). The enhancement of J_{SC} and η actually indicates that the branch structure of the TiO_2 NDs arrays has more surface area for $CuInS_2$ QDs adsorption. It is efficient for the electron injection to increase the photo-current than those of TiO_2 NPs based solar cells. The incident photon to current conversion efficiency (IPCE) spectra of the devices for these TiO_2 photo-anodes in Fig. 3b almost cover the whole ultraviolet and visible spectra within the range of 300–800 nm, which is well matched with the UV–vis spectra in Fig. 2a. The IPCE curves exhibit a maximum value of 25%, 38%, 30% and 42% for the r-TPs, a-TPs, TRs and TDs, respectively. And the average of IPCE spectra of TDs is larger than others. This result indicates that the structure of TiO_2 NDs arrays based solar cells has higher capability in inducing the photo-electrons. And it is more efficient

Table 1
Photovoltaic properties of the various $CuInS_2$ QDs sensitized solar cells.

Sample	J_{SC} (mA/cm^2)	V_{oc} (mV)	*FF* (%)	η (%)
TRs/heat	3.59	521.2	50.2	0.94
TDs/heat	4.70	528.7	50.7	1.26
a-TPs/heat	3.30	530.2	57.2	1.00
r-TPs/heat	2.74	521.3	58.1	0.83

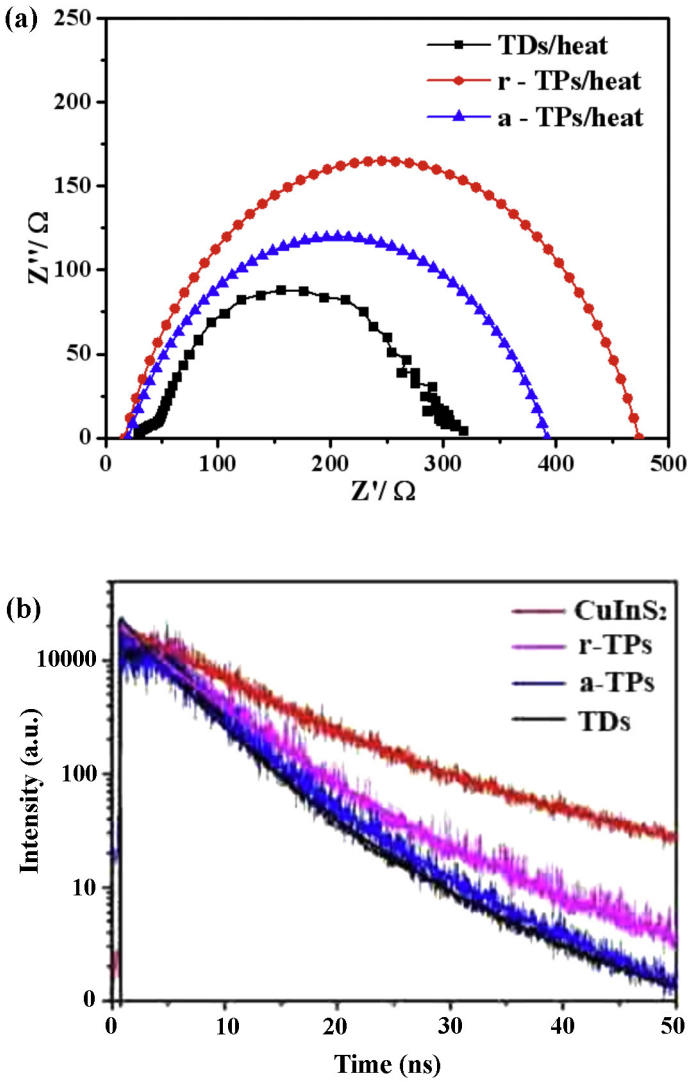

Fig. 4. (a) EIS spectra of $CuInS_2$ QDs sensitized solar cells with different TiO_2 photo-anodes and (b) photoluminescence decay of each device.

to reduce the electron–hole pairs' recombination to improve the charge separation and charge collection, which lead to the better photovoltaic performance.

3.4. Electrochemical impedance and photoluminescence decay analysis

Fig. 4a shows the semicircular curves of electrochemical impedance spectra (EIS) of above devices. It can be seen that the TiO_2 NPs have almost no first semicircle, which is lower than that of TiO_2 NDs, suggesting that the resistance between the TiO_2 and FTO substrate in TiO_2 NPs electrodes is lower. This result actually induces that the *FF* value of the TiO_2 NPs photo-anodes is higher than that of TiO_2 NDs, as shown in Table 1. It is attributed to the reduction of the interface combination between FTO substrate and TiO_2 nanodendrite with the length growth of the TiO_2 nanorod/nanodendrite. Actually it will induce some recombination between FTO and the electrolyte. However, the content of the QDs can be improved with the length increasing of the TiO_2 nanorod/nanodendrite. In order to balance these two factors, here we have prepared the 6 μm-TiO_2 nanorod/nanodendrite for the photo-anodes to obtain the better photovoltaic performance. However, the TiO_2 NDs based solar cells have the lowest second semicircular diameter than that of the other devices. This indicates that using the TiO_2 NDs array photo-anodes can obtain a lower resistance of photo-induced electron transfer among the $CuInS_2$ QDs, TiO_2 photo-anodes and electrolyte, which is attributed to the perfect mobility of charge carriers of the TiO_2 NDs, implying the higher J_{SC} value of the TiO_2 NDs photo-anodes. Therefore, this well-aligned three-dimensional TiO_2 NDs arrays structure can extensively decrease the barrier of electron transfer and accelerate the electron injection from $CuInS_2$ QDs to TiO_2, which improves the photovoltaic power conversion efficiency.

In order to gain the electron injection from this device, the photoluminescence decay is shown in Fig. 4b for $CuInS_2$, r-TPs, a-TPs and TDs, respectively. Normally, the PL decay will be influenced by the surface trapping events in the solar cells. However, in our work, the materials are not identical, as the colloidal $CuInS_2$ QDs are prepared by the presence of the MPA ligands, which were not prepared in situ process, and these colloidal $CuInS_2$ QDs are covered on the surface of TiO_2 films as the monolayer, which are connected with TiO_2 by the MPA ligands. Moreover, the $CuInS_2$ QDs without bonding with MPA molecules to the surface of TiO_2 will be washed and dispersed again in the solution, which will not be aggregated to influence the PL lifetime. Therefore, we believe that the surface trapping events are likely to be reduced in our work. From the Tri-exponential function model, the normalized PL decay parameters can be calculated using Eq. (1), as shown in Table 2. The value of average PL lifetime of each photo-anodes can be estimated using Eq. (2).

$$I = A_1 \exp\left(-\frac{t}{\tau_1}\right) + A_2 \exp\left(-\frac{t}{\tau_2}\right) + A_3 \exp\left(-\frac{t}{\tau_3}\right) \quad (1)$$

$$\tau_{av} = \frac{A_1\tau_1^2 + A_2\tau_2^2 + A_3\tau_3^2}{A_1\tau_1 + A_2\tau_2 + A_3\tau_3} \quad (2)$$

where τ_{av} is the average lifetime, $\alpha_n\tau_n$ are the each decay parameters of component in the multiexponential function model. When adsorbed on the FTO conducting substrate, the 3.5 nm $CuInS_2$ QDs exhibited PL emission decay with the average lifetime of 19.7 ns. When adsorbed on rutile TiO_2 NPs, anatase TiO_2 NPs and TiO_2 NDs, the average lifetime decrease from 19.7 ns to 11.7 ns, 7.9 ns and 7.4 ns, respectively. Thus it can be estimated the charge-transfer rate constant by the Eq. (3).

$$k_{et} = \frac{1}{\tau_{(CuInS_2+TiO_2)}} - \frac{1}{\tau_{(CuInS_2)}} \quad (3)$$

where k_{et} is the electron injection rate constants, $\tau_{(CuInS_2+TiO_2)}$ and $\tau_{(CuInS_2)}$ are the average lifetime of TiO_2/$CuInS_2$ photo-anodes and FTO/$CuInS_2$, respectively. From the PL lifetime value in Table 2, the apparent electron injection rate constants of r-TPs, a-TPs and TDs photo-anodes can be calculated through the lifetime values to be $3.39 \times 10^7\ s^{-1}$, $7.50 \times 10^7\ s^{-1}$ and $8.36 \times 10^7\ s^{-1}$, respectively. The electron injection rate constant of TDs photo-anodes is higher than that of r-TPs, a-TPs photo-anodes. Therefore, comparing the EIS and PL decay of the TiO_2 NDs and NPs, the much lower electrons transfer resistance and higher electron injection rate constant can indicate the more efficient of the electrons transfer for the TiO_2 NDs based solar cells. What's more, the QDs can be effectively deposited by the conventional SILAR method on the three-dimensional single crystal TiO_2 NDs due to its good interspace and surface area, while is easily limited and destroyed by the barrier as particle-to-particle of TiO_2 NPs photo-anode.

3.5. Mechanisms analysis

Fig. 5 proposes the use of a $CuInS_2$ QDs sensitized TiO_2 NDs arrays structure to enhance the quantity of electron transfer in

Table 2
Kinetic parameters of the $CuInS_2$ emission decay analysis.

Sample	A_1	τ_1 (ns)	A_2	τ_2 (ns)	A_3	τ_3 (ns)	τ_{av} (ns)	k_{ET} (s^{-1})
$CuInS_2$	0.72	12.06	0.51	29.30	0.05	43.40	19.7	–
r-TPs	0.77	6.25	0.49	17.72	0.12	20.94	11.7	3.39×10^7
a-TPs	0.68	4.43	0.37	10.75	0.11	11.17	7.9	7.50×10^7
TDs	0.58	2.57	0.41	9.39	0.09	14.35	7.4	8.36×10^7

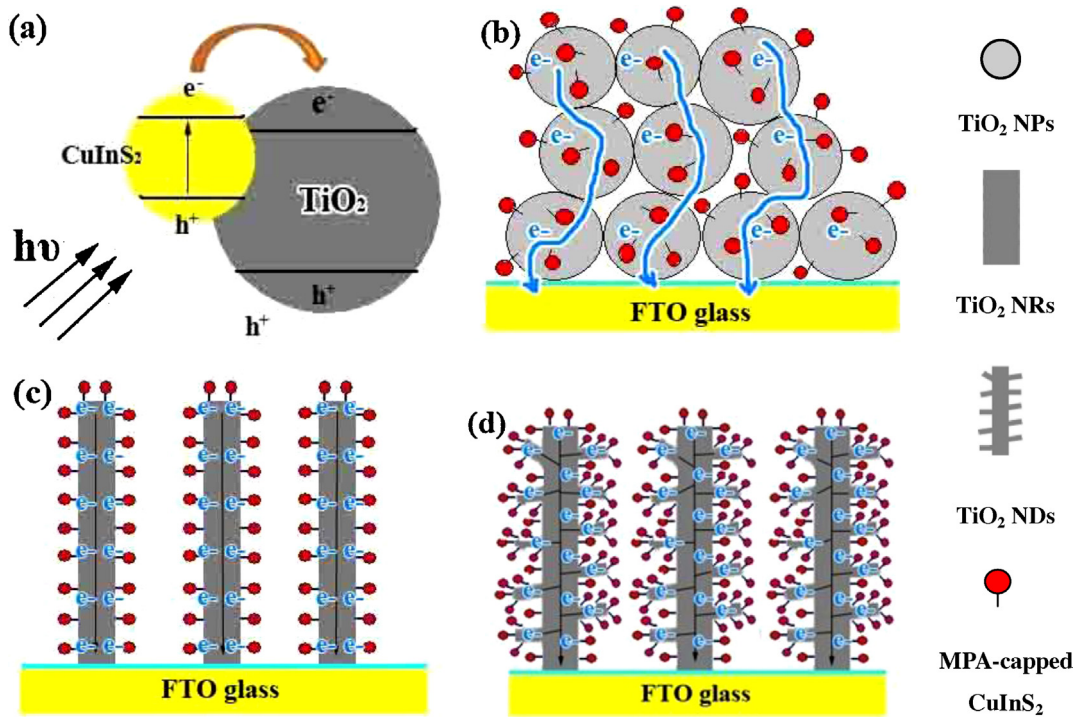

Fig. 5. Schematic diagram of $CuInS_2$ QDs sensitized solar cells: (a) band gap; electron transfer path of (b) TiO_2 nanoparticles, (c) TiO_2 nanorods and (d) TiO_2 nanodendrites sensitized with $CuInS_2$ QDs.

QDSSCs. The photovoltaic power conversion efficiency of the device in our proposed photo-anode structure has been enhanced comparing with the $CuInS_2/TiO_2$ NPs structure, even has great improvement for the current density. A schematic diagram of the electron transfer mechanism of photo-induced electron–holes is shown in Fig. 5a and each kind of $CuInS_2$ QDs sensitized TiO_2 solar cells with electron transfer is shown in Fig. 5b–d. Under 1.5 AM irradiation, the photo-induced electrons from $CuInS_2$ QDs are excited from the valence band to the conduction band of $CuInS_2$ QDs, and then injected into the conduction band of TiO_2 photo-anodes. Moreover, the photo-induced holes in $CuInS_2$ QDs will be scavenged by the electrolytes, which can effectively separate the photo-induced electron–holes. By using the photo-anodes of TiO_2 NPs in Fig. 5b, the photo-induced electrons excited from $CuInS_2$ QDs will transfer through the adjacent TiO_2 NPs, which may suffer from electron trapping at the grain boundaries of TiO_2 NPs. It will induce high charge recombination loss since the electron mobility. However, one-dimensional single crystal TiO_2 NRs/NWs arrays can obviously improve the electrons transfer by reducing the electron trapping, which may increase the possibility of electrons collection on the electrodes in Fig. 5c [32]. Comparatively, three-dimensional TiO_2 NDs arrays have much more branches on the surface of NRs/NWs, much more $CuInS_2$ QDs may be deposited to increase the higher generation possibility of the photo-induced electrons to improve the current density of the solar cells in Fig. 5d. Although the photovoltaic efficiency of the $CuInS_2$/CdS QDs co-sensitized solar cells have been achieved over 4% in the previous reports, the efficiencies of $CuInS_2$ QDSSCs are lower than that of our devices [14,15], and the $CuInS_2$ QDs sensitized TiO_2 NDs solar cells display the higher photovoltaic efficiency. It can be believed that further investigation of $CuInS_2$/CdS quantum dot co-sensitized TiO_2 nanodendrite array solar cells will obtain much higher efficiency of the solar cells.

4. Conclusions

In summary, the $CuInS_2$ QDs sensitized TiO_2 NDs array photo-anode have been successfully prepared for the QDSSCs. The single crystal TiO_2 NDs arrays have high surface area ratio, which can increase the deposition content of $CuInS_2$ QDs, inducing the improvement of the optical absorption properties and electro-hole separation of the photo-anode. The lower charge transfer resistance and shorter PL lifetime of the TiO_2 NDs based QDSSCs indicate the higher electron injection rate. The $CuInS_2$ QDs sensitized TiO_2 NDs arrays solar cells exhibits a photovoltaic power conversion efficiency of 1.26%. These devices show great improvement of J_{SC} if comparing to a QDs sensitized with TiO_2 NPs. We believe that the better electron transfer possibility of the TiO_2 NDs will facilitate improving the photovoltaic performance of QDSSCs.

Acknowledgements

This work is supported by the National Basic Research Program of China (No. 2009CB939704), Defense Industrial Technology Development Program (No. B1420110168), the National Nature Science Foundation of China (No. 51072152, the A3 Foresight Program-No. 51161140399), Educational Commission of Hubei

Province of China (No. C2010007), the Natural Science Foundation of Hubei Province (Key Program) (No. 2010CDA015), Wuhan Scientific and Technological Project (No. 201051730550), and Science-Technology Chenguang Foundation for Young Scientist of Wuhan (201150431087).

Appendix A. Supplementary data

Supplementary data associated with this article can be found, in the online version, at http://dx.doi.org/10.1016/j.electacta.2013.08.054.

References

[1] P.V. Kamat, K. Tvrdy, D.R. Baker, J.G. Radich, Beyond photovoltaics: semiconductor nanoarchitectures for liquid-junction solar cells, Chem. Rev. 110 (2010) 6664.
[2] Y.L. Lee, Y.S. Lo, Highly efficient quantum-dot-sensitized solar cell based on co-sensitization of CdS/CdSe, Adv. Funct. Mater. 19 (2009) 604.
[3] P.K. Santra, P.V. Kamat, Mn-doped quantum dot sensitized solar cells: a strategy to boost efficiency over 5%, J. Am. Chem. Soc. 134 (2012) 2508.
[4] Y.K. Lai, Z.Q. Lin, D.J. Zheng, L.F. Chi, R.G. Du, C.J. Lin, CdSe/CdS quantum dots co-sensitized TiO_2 nanotube array photoelectrode for highly efficient solar cells, Electrochim. Acta 79 (2012) 175.
[5] Y.Y. Yang, Q.X. Zhang, T.Z. Wang, L.F. Zhu, X.M. Huang, Y.D. Zhang, X. Hu, D.M. Li, Y.H. Luo, Q.B. Meng, Novel tandem structure employing mesh-structured Cu_2S counter electrode for enhanced performance of quantum dot-sensitized solar cells, Electrochim. Acta 88 (2012) 44.
[6] N. Balis, V. Dracopoulos, K. Bourikas, P. Lianos, Quantum dot sensitized solar cells based on an optimized combination of ZnS, CdS and CdSe with CoS and CuS counter electrodes, Electrochim. Acta 91 (2013) 246.
[7] H.H. Yang, W.G. Fan, A. Vaneski, A.S. Susha, W.Y. Teoh, A.L. Rogach, Heterojunction engineering of CdTe and CdSe quantum dots on TiO_2 nanotube arrays: intricate effects of size-dependency and interfacial contact on photoconversion efficiencies, Adv. Funct. Mater. 22 (2012) 2821.
[8] J. Tang, K.W. Kemp, S. Hoogland, K.S. Jeong, H. Liu, L. Levina, M. Furukawa, X.H. Wang, R. Debnath, D.K. Cha, K.W. Chou, A. Fischer, A. Amassian, J.B. Asbury, E.H. Sargent, Colloidal-quantum-dot photovoltaics using atomic-ligand passivation, Nat. Mater. 10 (2011) 765.
[9] A.N. Tiwari, D.K. Pandya, K.L. Chopra, Electrical and optical properties of single-phase $CuInS_2$ films prepared using spray pyrolysis, Thin Solid Films 130 (1985) 217.
[10] F. Hergert, R. Hork, S. Schorr, Pentanary chalcopyrite compounds without tetragonal deformation in the heptanary system Cu(Al, Ga, In)(S, Se, Te)$_2$, Sol. Energy Mater. Sol. Cells 91 (2007) 44.
[11] M. Bar, A. Ennaoui, J. Klaer, R.S. Araoz, T. Kropp, L. Weinhardt, C. Heske, H.W. Schock, C.H. Fischer, M.C. Steiner, The electronic structure of the [Zn(S,O)/ZnS]/$CuInS_2$ heterointerface – impact of post-annealing, Chem. Phys. Lett. 433 (2006) 71.
[12] Z.Y. Peng, Y.L. Liu, W. Shu, K.Q. Chen, W. Chen, Synthesis of various sized $CuInS_2$ quantum dots and their photovoltaic properties as sensitizers for TiO_2 photoanodes, Eur. J. Inorg. Chem. 32 (2012) 5239.
[13] P.K. Santra, P.V. Nair, K.G. Thomas, P.V. Kamat, $CuInS_2$-sensitized quantum dot solar cell. Electrophoretic deposition, excited-state dynamics, and photovoltaic performance, J. Phys. Chem. Lett. 4 (2013) 722.
[14] T.L. Li, Y.L. Lee, H.S. Teng, High-performance quantum dot-sensitized solar cells based on sensitization with $CuInS_2$ quantum dots/CdS heterostructure, Energy Environ. Sci. 5 (2012) 5315.
[15] J.H. Luo, H.Y. Wei, Q.L. Huang, X. Hu, H.F. Zhao, R.C. Yu, D.M. Li, Y.H. Luo, Q.B. Meng, Highly efficient core shell $CuInS_2$/Mn doped CdS quantum dots sensitized solar cells, Chem. Commun. 49 (2013) 3881.
[16] M. Grätzel, Photoelectrochemical cells, Nature 414 (2001) 338.
[17] W.W. Tan, X. Yin, X.W. Zhou, J.B. Zhang, X.R. Xiao, Y. Lin, Electrophoretic deposition of nanocrystalline TiO_2 films on Ti substrates for use in flexible dye-sensitized solar cells, Electrochim. Acta 54 (2009) 4467.
[18] B. Liu, E.S. Aydil, Growth of oriented single-crystalline rutile TiO_2 nanorods on transparent conducting substrates for dye-sensitized solar cells, J. Am. Chem. Soc. 131 (2009) 3985.
[19] J.G. Yu, J.J. Fan, L. Zhao, Dye-sensitized solar cells based on double-layered TiO_2 composite films and enhanced photovoltaic performance, Electrochim. Acta 55 (2010) 597.
[20] Q.X. Zhang, X.Z. Guo, X.M. Huang, S.Q. Huang, D.M. Li, Y.H. Luo, Q. Shen, T. Toyoda, Q.B. Meng, Highly efficient CdS/CdSe-sensitized solar cells controlled by the structural properties of compact porous TiO_2 photoelectrodes, Phys. Chem. Chem. Phys. 13 (2011) 4659.
[21] L.Y. Lin, M.H. Yeh, C.P. Lee, Y.H. Chen, R. Vittal, K.C. Ho, Metal-based flexible TiO_2 photoanode with titanium oxide nanotubes as the underlayer for enhancement of performance of a dye-sensitized solar cell, Electrochim. Acta 57 (2011) 270.
[22] K. Shankar, J.I. Basham, N.K. Allam, O.K. Varghese, G.K. Mor, X.J. Feng, M. Paulose, J.A. Seabold, K.S. Choi, C.A. Grimes, Recent advances in the use of TiO_2 nanotube and nanowire arrays for oxidative photoelectrochemistry, J. Phys. Chem. C 113 (2009) 6327.
[23] F. Shao, J. Sun, L. Gao, S.W. Yang, J.Q. Luo, Forest-like TiO_2 hierarchical structures for efficient dye-sensitized solar cells, J. Mater. Chem. 22 (2012) 6824.
[24] J.H. Bang, P.V. Kamat, Solar cells by design: photoelectrochemistry of TiO_2 nanorod arrays decorated with CdSe, Adv. Funct. Mater. 20 (2010) 1970.
[25] K.L. Li, Z.B. Xie, S. Adams, A reliable TiO_2 nanotube membrane transfer method and its application in photovoltaic devices, Electrochim. Acta 62 (2012) 116.
[26] I.S. Cho, Z.B. Chen, A.J. Forman, D.R. Kim, P.M. Rao, T.F. Jaramillo, X.L. Zheng, Branched TiO_2 nanorods for photoelectrochemical hydrogen production, Nano Lett. 11 (2011) 4978.
[27] W.P. Liao, J.J. Wu, Wet chemical route to hierarchical TiO_2 nanodendrite/nanoparticle composite anodes for dye-sensitized solar cells, J. Mater. Chem. 21 (2011) 9255.
[28] J.Y. Chang, L.F. Su, C.H. Li, C.C. Chang, J.M. Lin, Efficient “green” quantum dot-sensitized solar cells based on Cu_2S–$CuInS_2$–ZnSe architecture, Chem. Commun. 48 (2012) 4848.
[29] A. Hofmann, C. Pettenkofer, Surface orientation dependent band alignment for $CuInSe_2$–ZnSe–ZnO, App. Phys. Lett. 98 (2011) 113503.
[30] D.R. Pernik, K. Tvrdy, J.G. Radich, P.V. Kamat, Tracking the adsorption and electron injection rates of CdSe quantum dots on TiO_2: linked versus direct attachment, J. Phys. Chem. C 115 (2011) 13511.
[31] L. Brus, Electronic wave functions in semiconductor clusters: experiment and theory, J. Phys. Chem. 90 (1986) 2555.
[32] Y. Liu, H. Wang, Y.C. Wang, H.M. Xu, M. Li, H. Shen, Substrate-free, large-scale, free-standing and two-side oriented single crystal TiO_2 nanorod array films with photocatalytic properties, Chem. Commun. 47 (2011) 3790.